OPTIMAL CONTROL APPLICATIONS AND METHODS
Optim. Control Appl. Meth. 2015; **36**:968–984
Published online 19 January 2015 in Wiley Online Library (wileyonlinelibrary.com). DOI: 10.1002/oca.2159

Optimal spatial field control for controlled release‡

Masako Kishida[1,*,†], Daniel W. Pack[2] and Richard D. Braatz[3,4]

[1]*University of Canterbury, Christchurch 8140, New Zealand*
[2]*University of Kentucky, Lexington, KY 40506, USA*
[3]*Massachusetts Institute of Technology, Cambridge, MA 02139, USA*
[4]*University of Illinois at Urbana-Champaign, Champaign, IL 61801, USA*

SUMMARY

Most distributed parameter control problems involve manipulation within the spatial domain. Such problems arise in a variety of applications including epidemiology, tissue engineering, and cancer treatment. This paper proposes an approach to solve a state-constrained spatial field control problem that is motivated by a biomedical application. In particular, the considered manipulation over a spatial field is described by partial differential equations (PDEs) with spatial frequency constraints. The proposed optimization algorithm for tracking a reference spatial field combines three-dimensional Fourier series, which are truncated to satisfy the spatial frequency constraints, with exploitation of structural characteristics of the PDEs. The computational efficiency and performance of the optimization algorithm are demonstrated in a numerical example. In the example, the spatial tracking error is shown to be almost entirely due to the limitation on the spatial frequency of the manipulated field. The numerical results suggest that the proposed optimal control approach has promise for controlling the release of macromolecules in tissue engineering applications. Copyright © 2015 John Wiley & Sons, Ltd.

Received 22 July 2013; Revised 27 October 2014; Accepted 15 December 2014

KEY WORDS: optimization; optimal control; constraints; spatial field control; tissue engineering; spectral decomposition; distributed parameter systems

1. INTRODUCTION

In *spatial field control*, manipulation within a distributed parameter system (DPS) occurs as a spatial field. Spatial field control problems arise in a variety of applications including active control of communicable disease carriers [2], the engineering of biological tissues and organs [3], and cancer treatment [4]. The ability to manipulate within the spatial domain provides much more controllability than the heavily studied boundary control problems (e.g., [5]). On the other hand, the enhanced manipulation requires the determination of many more degrees of freedom. For example, for spatial field control problems with three spatial dimensions, the manipulated variable is a function of time and three spatial variables in domain, compared with boundary control in which manipulation is defined only on the external surface.

While many theoretical results have been derived for variety of classes of spatial field control problems [6–8], few contributions have proposed numerical algorithms that address all of the challenges that arise in real applications. Although nonlinear programming methods for solving optimal control problems such as control vector parameterization [9, 10] and direct transcription [11, 12]

*Correspondence to: Masako Kishida, Electrical and Computer Engineering Building, University of Canterbury, Private Bag 4800, Christchurch 8140, New Zealand.
†E-mail: masako.kishida@canterbury.ac.nz
‡A preliminary version appears in [1].

are directly applicable to boundary control and many other optimal control problems, spatial field control for real applications problems must be carefully formulated to arrive at a computationally feasible solution.

Consider, for example, an attempt to solve a simple open-loop spatial field control problem using control vector parameterization with a standard finite-difference discretization of a single partial differential equation (PDE) over time and the three spatial dimensions with 100 grid points in each dimension. The resulting nonlinear program with $100^4 = 10^8$ optimization variables is too computationally complex to be solved with existing computer hardware and software. The spatial control problems that arise in real applications can be more complicated, involving multiple PDEs and typically requiring the satisfaction of spatial constraints on the state or manipulated fields.

This paper addresses a state-constrained spatial field control problem for a system described by tightly coupled PDEs. As is common in the optimal control of PDEs, basis function expansions are used to reduce the number of degrees of freedom to a manageable size [1, 13–15]. As the basis function, this paper uses Fourier sine series, which results from the spectral decomposition of the system. Instead of problem-independent basis functions such as Legendre polynomials, radial basis functions, and proper orthogonal decomposition that have become very popular in the last decade or so [16–20], basis functions arising from spectral decomposition are used to reduce computational complexity. The methodology is presented in the context of a spatial field control problem motivated by tissue engineering [3, 21–25], in which a molecular species is released within a biological tissue from fixed embedded polymer microparticles designed to provide controlled release [26, 27]. The transport of the molecular species is described by reaction–diffusion–convection equations in three spatial dimensions, and the control problem is to provide a desired spatial and temporal uptake of the molecular species throughout the biological tissue. The reader is directed to a past article [3] for additional details on the biological motivation for the optimal control problem, including additional references to relevant tissue engineering literature.

2. MATHEMATICAL NOTATION

For brevity purposes, this paper uses the notations:

$$\Omega := [0,\ 1] \times [0,\ 1] \times [0,\ 1], \tag{1}$$

$$\int_{\Omega} f(\cdot) dV := \int_0^1 \int_0^1 \int_0^1 f(\cdot) dx dy dz, \tag{2}$$

$$\int_{\Omega} f(\cdot) d\bar{V} := \int_0^1 \int_0^1 \int_0^1 f(\cdot) d\bar{x} d\bar{y} d\bar{z}, \tag{3}$$

$$\sum^{MNL} := \sum_{m=1}^{M} \sum_{n=1}^{N} \sum_{l=1}^{L}, \tag{4}$$

$$\sum_{-MNL}^{MNL} := \sum_{m=-M}^{M} \sum_{n=-N}^{N} \sum_{l=-L}^{L}, \tag{5}$$

$$\sum^{\infty} := \sum_{m=1}^{\infty} \sum_{n=1}^{\infty} \sum_{l=1}^{\infty}, \tag{6}$$

$$\sum_{-\infty}^{\infty} := \sum_{m=-\infty}^{\infty} \sum_{n=-\infty}^{\infty} \sum_{l=-\infty}^{\infty}, \tag{7}$$

DOI: 10.1002/oca

$$\sum_{+1}^{\infty} := \sum_{m=M+1}^{\infty} \sum_{n=N+1}^{\infty} \sum_{l=L+1}^{\infty} . \tag{8}$$

3. SPATIAL FIELD CONTROL PROBLEM

This paper considers a system where a molecular species is initially located in small biostable biocompatible polymer microparticles that are embedded in a tissue scaffold along with cells [24, 25]. Over time, the molecules are released from the microparticles and taken up by the surrounding cells, which cause the cells to change their behavior. The control objective is to provide a desired spatial and temporal cellular uptake rate, which is related to the local molecular species concentration.

The model consists of two kinds of systems that are interconnected (Figure 1). System 1 is a microparticle, which is a microscopic system with molecular species diffusing within the microparticle. System 2 is the tissue construct, in which a large number of microparticles are embedded. System 2 is a macroscopic system that describes the dynamics of the molecular species within the tissue construct as the molecules diffuse, convect because of fluid flow, and are consumed by the cells. System 1 locally provides the manipulation to System 2, or in other words, System 1 determines the source term for System 2. The collection of System 1 consists of a large number of microparticles and is treated as a continuum with respect to System 2, that is, each point in the macroscopic space is associated with several microparticles that determine the source of that point. This continuum assumption is most accurate for length scales larger than the diameter of a cell (about 10 μm). Also, the effective transport due to Brownian motion is assumed to be spatially uniform for both systems.

System 1

Each polymer microparticle is assumed to consist of a polymer core that initially contains a uniform concentration of molecular species to be released and a polymer shell that initially does not contain the molecular species. The inclusion of a polymer shell provides a much greater variety of release rates than microspheres, including the creation of a delay in the release profile [26]. Technology is available for manufacturing these core-shell microparticles to have precisely specified physical properties [26].

The transport of species through a biostable and biocompatible polymeric core-shell microparticle is described by a PDE for the concentration field of the species in the microparticle, $C_r(r, x, y, z, t)$,

$$\frac{\partial C_r}{\partial t} = \kappa \left(\frac{\partial^2 C_r}{\partial r^2} + \frac{2}{r} \frac{\partial C_r}{\partial r} \right), \quad t > t_p, \quad 0 \leqslant r < R_p, \tag{9}$$

with initial condition

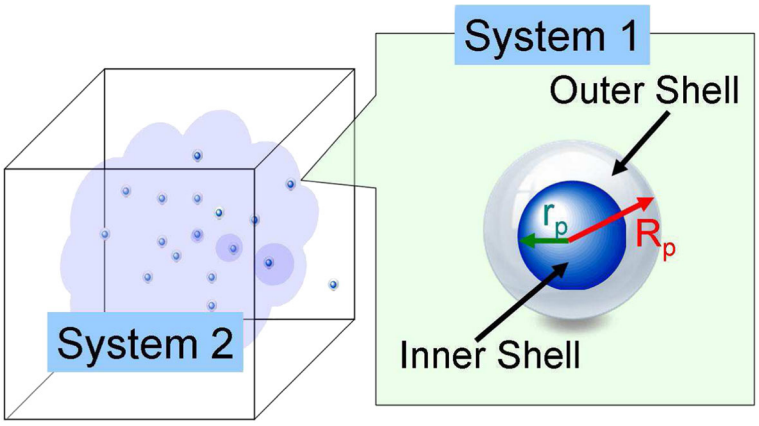

Figure 1. Overview of the system.

DOI: 10.1002/oca

$$C_r(r,x,y,z,t_p) = \begin{cases} C_{r0}(x,y,z), & 0 \leqslant r < r_p, \\ 0, & r_p \leqslant r < R_p, \end{cases} \tag{10}$$

and boundary conditions

$$\left.\frac{\partial C_r}{\partial r}\right|_{r=0} = 0, \tag{11}$$

$$C_r(R_p,x,y,z,t) = k_p C(x,y,z,t), \tag{12}$$

where $\kappa > 0$ is the effective diffusion coefficient within the core-shell microparticle, which is assumed to be the same in the polymer core and polymer shell and can be modified by changing the polymer chemistry, molecular weight distribution, porosity, or tortuosity [28], r_p is the radius of the polymer core, R_p is the outer radius, k_p is the partition coefficient that can be modified by changing the polymer chemistry, and t_p is the time for which the core-shell microparticles are activated by a spatially uniform environmental trigger. Regarding t_p, many environmental triggers have been demonstrated in tissue engineering applications, including pH, temperature, pressure, light, glucose, electric current, ultrasound, magnetic field, enzymes and other proteins, and ionic strength [29–33]. These environmental triggers can be activated with spatial uniformity across the biological tissue. $C(x,y,z,t)$ is the molecular species concentration field in the engineered tissue construct, and C and C_r are concentrations of the same molecular species. Equation (12) relates the concentration at the microparticle boundary to the macroscopic concentration.

To simplify manufacturing of the tissue construct, the core-shell microparticles are assumed to be identical except for having different initial loading C_{r0}. The spatial variation is constrained because of manufacturing and restricted to lower spatial frequencies, given in terms of M, N, and L as

$$C_{r0}(x,y,z) = \sum_{-MNL}^{MNL} C_{r0,mnl} e^{(m\pi x + n\pi y + l\pi z)i} \tag{13}$$

for some complex numbers $C_{r0,mnl}$ for $-M \leqslant m \leqslant M$, $-N \leqslant n \leqslant N$ and $-L \leqslant l \leqslant L$.[‡]

Interconnection

The manipulated field $u(x,y,z,t)$ represents the flux of the species from the microparticles into the tissue and is related to the core-shell microparticles by

$$u(x,y,z,t) = 4\pi\rho R_p^2 J\big|_{r=R_p}, \tag{14}$$

where $4\pi R_p^2$ is the external surface area and ρ is the number density (the number of microparticles per unit volume) of the core-shell microparticles. The flux at the surface of a single core-shell microparticle is

$$J|_{r=R_p} = -\kappa \left.\frac{\partial C_r}{\partial r}\right|_{r=R_p}. \tag{15}$$

Here, the system is continuous in the sense that each point in the spatial domain is associated with a number density of microparticles. Technology exists for embedding a specified spatial distribution of such microparticles within a tissue matrix [34, 35]. Changing the number density has exactly the same effect on the spatiotemporal release as changing the initial loading, so the number density ρ is assumed to be spatially uniform in (x,y,z) without changing the achievable value for the control objective.

[‡]The complex numbers $C_{r0,mnl}$ will be selected so that $C_{r0}(x,y,z)$ is real.

DOI: 10.1002/oca

System 2

The concentration field $C(x, y, z, t)$ in the engineered tissue construct is modeled by the reaction–diffusion–convection equation,

$$\frac{\partial C}{\partial t} = D\nabla^2 C - v \cdot \nabla C - g(C) + u(x, y, z, t), \ \forall t > 0, (x, y, z) \in \Omega, \tag{16}$$

which is a parabolic PDE with manipulated field $u(x, y, z, t)$ representing the flux of the molecular species from the microparticles into the tissue, $D > 0$ is the effective diffusion coefficient, v is the spatially uniform velocity vector field, Ω is the spatial domain as the unit cube (1), and $g(C)$ is the net species consumption by cellular uptake and species degradation. The effects of the molecular species reversibly binding with the extracellular matrix can be included with minor modifications of the model. To simplify the presentation, assume the zero initial condition

$$C(x, y, z, t) = 0, \ t \leqslant t_p, \tag{17}$$

and the Dirichlet boundary condition

$$C(x, y, z, t) = 0 \ \text{ on } \ \partial\Omega. \tag{18}$$

Control Objective

The control objective is to provide a desired spatial and temporal cellular uptake rate, which is related to the local molecular species concentration by

$$R_{uptake}(x, y, z, t) = f_{uptake}(C(x, y, z, t)), \tag{19}$$

where f_{uptake} is an invertible algebraic function that can be identified from *in vitro* cell culture experiments [36, 37]. To simplify the mathematical formulation, (19) is inverted to derive an expression for a reference concentration field

$$C_d(x, y, z, t) = f_{uptake}^{-1}\left(R_{uptake,des}(x, y, z, t)\right), \tag{20}$$

for the desired cellular uptake rate $R_{uptake,des}(x, y, z, t)$ so that the mathematical control objective is to determine properties of the polymer microparticles that minimize the error between the reference and model species concentration fields. The reference concentration field $C_d(x, y, z, t)$ is assumed to be continuously differentiable in time and twice continuously differentiable in the spatial directions and satisfies the zero initial condition

$$C_d(x, y, z, t) = 0, \ t \leqslant 0 \tag{21}$$

and the Dirichlet boundary condition

$$C_d(x, y, z, t) = 0 \ \text{ on } \ \partial\Omega. \tag{22}$$

The spatial field control problem is to determine the optimal properties of the polymer microparticles

$$\{\rho, R_p, r_p, k_p, \kappa, t_p, C_{r0}(x, y, z)\} \tag{23}$$

that specify a manipulated field $u(x, y, z, t)$ of constrained spatial variation that minimizes the error between the reference and model species concentration fields,

$$E = \int_T \int_\Omega (C_d(x, y, z, t) - C(x, y, z, t))^2 dV dt, \tag{24}$$

where $T = [t_0, t_f]$ is the time range of interest with the final time t_f and the initial time $t_0 = \min\{0, t_p\}$. A negative t_p allows the microparticles to be activated to give a nonzero manipulated field $u(x, y, z, t)$ for negative t, while the reference field $C_d(x, y, z, t)$ is zero. The objective function (24) takes into account the error during $t_p < t < 0$.

DOI: 10.1002/oca

4. OPTIMIZATION IN THE OUTPUT FIELD

This section considers the case where there is no convection term and reaction term is linear in the concentration for System 2.

4.1. Case I: $v = 0$, $g(C) = kC$, $k_p = 0$

For a system with no convection, linear uptake kinetics $g(C) = kC$ for some k and zero partition coefficient, the set of optimization variables is

$$\{\rho, R_p, r_p, \kappa, t_p, C_{r0}(x, y, z)\}. \tag{25}$$

By applying separation of variables [38] with $k_p = 0$ and $t_p = 0$ (the case of a nonzero time shift is introduced later), the analytical solution to the microparticle equations (9)–(12) is

$$C_r(r, x, y, z, t) = \frac{2C_{r0}(x, y, z)}{r} \sum_{j=1}^{\infty} \frac{r_p}{j\pi} \sin \frac{j\pi r}{R_p} \underbrace{e^{-\frac{\kappa j^2 \pi^2}{R_p^2} t} \left(\frac{R_p}{j\pi r_p} \sin \frac{j\pi r_p}{R_p} - \cos \frac{j\pi r_p}{R_p} \right)}_{=:w_j(t)}. \tag{26}$$

Inserting this equation into (15) gives the flux at the microparticle surface,

$$J\Big|_{r=R_p} = \frac{2\kappa r_p C_{r0}(x, y, z)}{R_p^2} \underbrace{\sum_{j=1}^{\infty} (-1)^{j+1} w_j(t)}_{=:w(t)}, \tag{27}$$

which inserted into (14) gives the manipulated field

$$u(x, y, z, t) = 8\pi\rho\kappa r_p C_{r0}(x, y, z) w(t). \tag{28}$$

To remove redundancy in the optimization variables, define

$$\alpha(x, y, z) := 8\pi\rho\kappa r_p C_{r0}(x, y, z), \tag{29}$$

$$\beta := \frac{r_p}{R_p}, \tag{30}$$

$$\gamma := \frac{\kappa}{R_p^2}, \tag{31}$$

then

$$w_j(t) = \begin{cases} e^{-\gamma j^2 \pi^2 t} \left(\frac{\sin j\pi\beta}{j\pi\beta} - \cos j\pi\beta \right), & t \geqslant 0 \\ 0, & t < 0, \end{cases} \tag{32}$$

and

$$u(x, y, z, t) = \alpha(x, y, z) w(t). \tag{33}$$

These expressions indicate that the optimization in the spatial component depends only on α, and the temporal component depends only on β and γ. Equations (29)–(31) are used throughout the rest of this paper.

For $v = 0$ and $g(C) = kC$, the cosine terms in (13) do not contribute to the concentration field C because the eigenfunctions of the system are sine functions. Hence, the parameter α that satisfies the spatial frequency constraints on the manipulated field can be written as a truncated Fourier sine series

DOI: 10.1002/oca

$$\alpha(x,y,z) = \sum^{MNL} \alpha_{mnl} \sin m\pi x \sin n\pi y \sin l\pi z =: \alpha_{MNL}(x,y,z), \tag{34}$$

where the real 3D Fourier sine series coefficients α_{mnl} are to be determined. Insertion into (33) results in the manipulated field

$$u(x,y,z,t) = \alpha_{MNL}(x,y,z)w(t). \tag{35}$$

Expressions for the manipulated field (34) and the Green's function G of (16) with $v = 0$ [39] can be used to derive an analytical solution for the concentration field:

$$\begin{aligned} C(x,y,z,t) &= \int_0^t \int_\Omega u(\bar{x},\bar{y},\bar{z},\tau) G(x,y,z,\bar{x},\bar{y},\bar{z},t-\tau)\, d\bar{V}\, d\tau \\ &= \sum^{MNL} \alpha_{mnl} c_{mnl}(t) \sin m\pi x \sin n\pi y \sin l\pi z \end{aligned} \tag{36}$$

where

$$\begin{aligned} G(x,y,z,\bar{x},\bar{y},\bar{z},t) = 8 \sum_{}^{\infty} & e^{-(D(m^2+n^2+l^2)\pi^2+k)t} \\ & \times \sin m\pi x \sin n\pi y \sin l\pi z \sin m\pi \bar{x} \sin n\pi \bar{y} \sin l\pi \bar{z} \end{aligned} \tag{37}$$

and

$$c_{mnl}(t) = \sum_{j=1}^{\infty} \frac{1 - e^{-((D(m^2+n^2+l^2)-\gamma j^2)\pi^2+k)t}}{(D\,(m^2+n^2+l^2) - \gamma j^2)\,\pi^2 + k} (-1)^{j+1} w_j(t). \tag{38}$$

The reference field C_d written in terms of the 3D Fourier series (also known as its spectral decomposition [40]) is a Fourier sine series with the given boundary condition (18),

$$C_d(x,y,z,t) = \sum_{}^{\infty} c_{d,mnl}(t) \sin m\pi x \sin n\pi y \sin l\pi z, \tag{39}$$

where

$$c_{d,mnl}(t) = 8 \int_\Omega C_d(x,y,z,t) \sin m\pi x \sin n\pi y \sin l\pi z\, dV. \tag{40}$$

By taking into account a potentially nonzero trigger time t_p, the optimization (24) can be written equivalently as, by application of orthogonality,

$$\begin{aligned} \min_{\alpha_{mnl},\beta,\gamma,t_p} E \Leftrightarrow \min_{\alpha_{mnl},\beta,\gamma,t_p} & \sum^{MNL} \int_{t_0}^{t_f} \left(c_{d,mnl}(t) - \alpha_{mnl} c_{mnl}(t-t_p)\right)^2 dt \\ & + \sum_{+1}^{\infty} \int_{t_0}^{t_f} \left(c_{d,mnl}(t)\right)^2 dt. \end{aligned} \tag{41}$$

Note that $c_{d,mnl}(t) = 0, \forall t \leqslant 0$ and recall that t_f is the final time of interest and $t_0 = \min\{0, t_p\}$. This previous analysis reduces the set of optimization variables to

$$\{\alpha_{mnl}, \beta, \gamma, t_p\}, \tag{42}$$

where α_{mnl} is the (m,n,l) 3D Fourier series coefficient of $\alpha(x,y,z)$.

DOI: 10.1002/oca

The optimization (41) is largely decoupled and is solved by a combination of gridding and analytical methods:

1. grid β, γ, and t_p over ranges that are guaranteed to include the global solution,
2. for each combination of these parameter values, analytically determine the optimal α_{mnl} for each m, n, and l (the expressions are given in the succeeding text),
3. calculate and store the value of the optimization objective E,
4. repeat Steps 2 and 3 for each grid point,
5. select the minimum E for all grid points, and
6. refine the grid until the optimal objective no longer reduces significantly.

An initial estimate for the trigger time t_p can be obtained by first solving the optimization for $t_p = 0$ and then shifting t_p by the difference in the times in which the maximum desired and achieved concentration fields occur. The optimization over α_{mnl} in Step 2 is convex and so can be determined by basic calculus as

$$\alpha_{mnl} = \frac{\int_{t_0}^{t_f} c_{d,mnl}(t) c_{mnl}(t - t_p) dt}{\int_{t_0}^{t_f} \left(c_{mnl}(t - t_p)\right)^2 dt}. \tag{43}$$

For initial ranges for β, γ, and t_p that include the global minimum, the convexity of the optimization over α_{mnl} and the continuity of the solution of the PDEs as a function of the optimization parameters imply that the optimization algorithm will converge within any specific tolerance to the global optimum.

4.2. *Case II:* $v = 0$, $g(C) = kC$, $k_p \neq 0$

For a system with no convection, linear uptake kinetics $g(C) = kC$ and a nonzero partition coefficient, the set of optimization variables is again

$$\left\{\rho, R_p, r_p, \kappa, t_p, C_{r0}(x, y, z)\right\}. \tag{44}$$

The analytical solution to the microparticle equations (9)–(12) is

$$\begin{aligned} C_r(r, x, y, z, t) = {} & \frac{2C_{r0}(x, y, z)}{r} \sum_{j=1}^{\infty} \frac{r_p}{j\pi} \sin \frac{j\pi r}{R_p} w_j(t) \\ & + \frac{2\kappa k_p}{rR_p} \sum_{j=1}^{\infty} \sin \frac{j\pi r}{R_p} (-1)^{j+1} j\pi \int_0^t C(x, y, z, \tau) e^{-\gamma j^2 \pi^2 (t-\tau)} d\tau, \end{aligned} \tag{45}$$

and the flux at the microparticle surface from (15) is

$$J|_{r=R_p} = \frac{2\kappa r_p C_{r0}(x, y, z)}{R_p^2} w(t) + \frac{2\kappa^2 k_p}{R_p^3} \sum_{j=1}^{\infty} (j\pi)^2 \int_0^t C(x, y, z, \tau) e^{-\gamma j^2 \pi^2 (t-\tau)} d\tau, \tag{46}$$

which inserted into (14) gives the manipulated field:

$$\begin{aligned} u(x, y, z, t) &= 8\pi\kappa\rho r_p C_{r0}(x, y, z) w(t) + \frac{8\pi\kappa^2 \rho k_p}{R_p} \sum_{j=1}^{\infty} (j\pi)^2 \int_0^t C(x, y, z, \tau) e^{-\gamma j^2 \pi^2 (t-\tau)} d\tau \\ &= \alpha(x, y, z) w(t) + \delta \sum_{j=1}^{\infty} (j\pi)^2 \int_0^t C(x, y, z, \tau) e^{-\gamma j^2 \pi^2 (t-\tau)} d\tau, \end{aligned} \tag{47}$$

DOI: 10.1002/oca

where

$$\delta := \frac{8\pi\kappa^2\rho k_p}{R_p}. \tag{48}$$

By choosing the initial loading in terms of a truncated Fourier sine series, the output field is also expressed by a truncated Fourier sine series, that is,

$$C(x,y,z,t) = \sum^{MNL} \bar{c}_{mnl}(t)\sin m\pi x \sin n\pi y \sin l\pi z \tag{49}$$

for some $\bar{c}_{mnl}$. Because most of the error in (41) is due to the spatial constraint (we will see this in the numerical example),

$$\bar{c}_{mnl}(t) \approx c_{d,mnl}(t). \tag{50}$$

By using this approximation,

$$u(x,y,z,t) = \sum^{MNL} u_{mnl}(t)\sin m\pi x \sin n\pi y \sin l\pi z, \tag{51}$$

where

$$u_{mnl}(t) \approx \alpha_{mnl} w(t) + \delta \sum_{j=1}^{\infty} (j\pi)^2 \int_0^t c_{d,mnl}(\tau) e^{-\gamma j^2\pi^2(t-\tau)} d\tau, \tag{52}$$

and the output field is

$$\begin{aligned} C(x,y,z,t) &= \int_0^t \int_\Omega u(\bar{x},\bar{y},\bar{z},\tau) G(x,y,z,\bar{x},\bar{y},\bar{z},t-\tau) d\bar{V} d\tau \\ &= \sum^{MNL} \tilde{c}_{mnl}(t)\sin m\pi x \sin n\pi y \sin l\pi z, \end{aligned} \tag{53}$$

where

$$\tilde{c}_{mnl}(t) = \alpha_{mnl} \underbrace{\int_0^t w(\tau) e^{-(D(m^2+n^2+l^2)\pi^2+k)(t-\tau)} d\tau}_{=c_{mnl}(t) \text{ as in (38)}} + \tilde{c}_{d,mnl}(t), \tag{54}$$

and

$$\tilde{c}_{d,mnl}(t) = \delta \sum_{j=1}^{\infty} (j\pi)^2 \int_0^t \int_0^\tau c_{d,mnl}(\bar{\tau}) e^{-\gamma j^2\pi^2(\tau-\bar{\tau})} d\bar{\tau} e^{-(D(m^2+n^2+l^2)\pi^2+k)(t-\tau)} d\tau. \tag{55}$$

The optimization strategy is similar to Case I. By taking into account a potentially nonzero trigger time t_p, the optimization (24) becomes, by application of orthogonality,

$$\min_{\alpha_{mnl},\beta,\gamma,\delta,t_p} E \Leftrightarrow \min_{\alpha_{mnl},\beta,\gamma,\delta,t_p} \sum^{MNL} \int_{t_0}^{t_f} \left(c_{d,mnl}(t) - \alpha_{mnl} c_{mnl}(t-t_p) - \tilde{c}_{d,mnl}(t)\right)^2 dt. \tag{56}$$

Note that $c_{d,mnl}(t) = 0$, $\forall t \leqslant 0$ and recall that t_f is the final time of interest and $t_0 = \min\{0, t_p\}$. These steps reduce the set of optimization variables to

$$\{\alpha_{mnl}, \beta, \gamma, \delta, t_p\}. \tag{57}$$

DOI: 10.1002/oca

The optimization (56) is largely decoupled and is solved by a combination of gridding and analytical methods:

1. grid β, γ, δ, and t_p over ranges that are guaranteed to include the global solution,
2. for each combination of these parameter values, determine the optimal α_{mnl} for each m, n, and l (this can be performed analytically, as discussed in the succeeding paragraphs),
3. calculate and store the value of the optimization objective E,
4. repeat Steps 2 and 3 for each grid point,
5. select the minimum E for all grid points, and
6. refine the grid until the optimal objective no longer reduces significantly.

The optimization over α_{mnl} in Step 2 is again convex and so can be determined by basic calculus as

$$\alpha_{mnl} = \frac{\int_{t_0}^{t_f} \left(c_{d,mnl}(t) - \tilde{c}_{d,mnl}(t)\right) c_{mnl}(t - t_p)dt}{\int_{t_0}^{t_f} c_{mnl}(t - t_p)^2 dt}. \tag{58}$$

As before, for initial ranges for β, γ, δ, and t_p that include the global minimum, the optimization algorithm will converge within any specific tolerance of the global optimum.

5. OPTIMIZATION IN THE MANIPULATED FIELD

This section briefly describes optimization in the manipulated field, which is useful if the computational cost is expensive when trying to minimize the error in the concentration field as defined in (24). Such cases include when $g(C)$ is nonlinear, where analytical solution to (16) is not possible, or when there is a convection term, that is, $v \neq 0$, where the solution to the PDE (16) is no longer a Fourier sine series and orthogonality cannot be used in (41).

5.1. Justification

For a given PDE (16) and a reference field C_d, let

$$\bar{u}(x, y, z, t) = \arg\min_{\mathcal{A}} \int_T \int_\Omega (C_d(x, y, z, t) - C(x, y, z, t))^2 dV dt, \tag{59}$$

$$\hat{u}(x, y, z, t) = \arg\min_{\mathcal{B}} \int_T \int_\Omega (C_d(x, y, z, t) - C(x, y, z, t))^2 dV dt, \tag{60}$$

where

- $\mathcal{A}$ is the set of functions $u(x, y, z, t)$ that satisfies the spatial frequency constraint

$$u(x, y, z, t) = \sum_{-MNL}^{MNL} u_{mnl}(t) e^{(m\pi x + n\pi y + l\pi z)i}, \tag{61}$$

- $\mathcal{B}$ is the set of functions $u(x, y, z, t)$ produced by System 1 with design parameters (25) that satisfy the spatial frequency constraint (13).

Recall that C_d is continuously differentiable in time and twice continuously differentiable in the spatial directions, and let

$$u_{des}(x, y, z, t) := \frac{\partial C_d}{\partial t} - D\nabla^2 C_d + v \cdot \nabla C_d + g(C_d), \tag{62}$$

then

$$C_d(x, y, z, t) := G(u_{des}), \tag{63}$$

DOI: 10.1002/oca

where G is a nonlinear map that maps the input u to the solution to the PDE (16). Note that (62) defines u_{des} only for $t > 0$, but it is a perfect control under the assumption that C_d is zero for time $t \leqslant 0$ as in (21). Similarly, write

$$\bar{C}(x, y, z, t) = G(\bar{u}) \tag{64}$$

$$\hat{C}(x, y, z, t) = G(\hat{u}). \tag{65}$$

Then the minimum error between the reference and concentration fields over the optimization parameters can be bounded previously as follows:

$$\begin{aligned} E &= \int_T \int_\Omega \left(C_d(x, y, z, t) - \hat{C}(x, y, z, t) \right)^2 dVdt \\ &= \int_T \int_\Omega \left(G(u_{des}) - G(\bar{u}) + G(\bar{u}) - G(\hat{u}) \right)^2 dVdt \\ &\leqslant 2 \underbrace{\int_T \int_\Omega \left(G(u_{des}) - G(\bar{u}) \right)^2 dVdt}_{\text{error due to spatial constraint}} + 2 \underbrace{\int_T \int_\Omega \left(G(\bar{u}) - G(\hat{u}) \right)^2 dVdt}_{\text{error due to physics of System 1}}. \end{aligned} \tag{66}$$

Note that $C(x, y, z, t)$ in (24) is replaced by $\hat{C}(x, y, z, t)$ because the optimal concentration is due to $\hat{u}$ by definition (65). The error due to the spatial constraint is a manufacturing limit that cannot be made smaller, which motivates the minimization of the error in the last term of (66). Assuming that the solution to the PDE depends continuously on the manipulated field, it is motivated to minimize the error in the manipulated field

$$\int_T \int_\Omega (\bar{u} - \hat{u})^2 \, dVdt. \tag{67}$$

In fact, if $g(C)$ is linear, by Young's inequality for convolutions, error due to physics of System 1 is bounded previously as follows;

$$\begin{aligned} \int_T \int_\Omega \left(G(\bar{u}) - G(\hat{u}) \right)^2 dVdt &= \int_T \int_\Omega \left(G \circ \bar{u} - G \circ \hat{u} \right)^2 dVdt \\ &\leqslant \left(\int_T \int_\Omega |G| dVdt \right)^2 \int_T \int_\Omega (\bar{u} - \hat{u})^2 \, dVdt, \end{aligned}$$

where $\circ$ denotes the convolution, and G becomes an appropriate Green's function.

5.2. *Case I:* $k_p = 0$

For zero partition coefficient, $u_{des}(x, y, z, t)$ in (62) gives a perfect control to System 2. Under the spatial constraint,

$$u_{des}(x, y, z, t) = \sum_{-\infty}^{\infty} u_{des,mnl}(t) e^{(m\pi x + n\pi y + l\pi z)i}, \tag{68}$$

where

$$u_{des,mnl}(t) = \int_\Omega u_{des}(x, y, z, t) e^{-(m\pi x + n\pi y + l\pi z)i} \, dV, \tag{69}$$

is truncated to

DOI: 10.1002/oca

$$u_{des,MNL}(x,y,z,t) = \sum_{-MNL}^{MNL} u_{des,mnl}(t) e^{(m\pi x + n\pi y + l\pi z)i} = \bar{u}(x,y,z,t). \tag{70}$$

On the other hand, from (13), (14), (15), and (29), any manipulated field that is produced by System 1 with the spatial constraint is in the form of

$$u_{MNL}(x,y,z,t) = \sum_{-MNL}^{MNL} \alpha_{mnl} e^{(m\pi x + n\pi y + l\pi z)i} w(t). \tag{71}$$

By substituting (70) and (71) into (67),

$$\begin{aligned}
&\int_T \int_\Omega (\bar{u} - \hat{u})^2 \, dV dt \\
&= \int_{t_0}^{t_f} \int_\Omega \left(\sum_{-MNL}^{MNL} \left(u_{des,mnl}(t) - \alpha_{mnl} w(t - t_p) \right) e^{-(m\pi x + n\pi y + l\pi z)i} \right)^2 dV dt \\
&\leqslant 8MNL \int_{t_0}^{t_f} \int_\Omega \sum_{-MNL}^{MNL} \left| \left(u_{des,mnl}(t) - \alpha_{mnl} w(t - t_p) \right) e^{-(m\pi x + n\pi y + l\pi z)i} \right|^2 dV dt \\
&\leqslant 8MNL \sum_{-MNL}^{MNL} \int_{t_0}^{t_f} \left| \left(u_{des,mnl}(t) - \alpha_{mnl} w(t - t_p) \right) \right|^2 dt \int_\Omega \left| e^{-(m\pi x + n\pi y + l\pi z)i} \right|^2 dV \\
&= 8MNL \sum_{-MNL}^{MNL} \int_{t_0}^{t_f} \left| u_{des,mnl}(t) - \alpha_{mnl} w(t - t_p) \right|^2 dt.
\end{aligned} \tag{72}$$

If the right-hand side of (72) becomes small, the error in the manipulated field (67) also becomes small. Note that $u_{des,mnl}(t)$ is already known from the reference field $C_d(x,y,z,t)$, and $w(t-t_p)$ is known for a fixed dynamics of System 2 and t_p. By replacing the objective function by the right-hand side of the previous equation, the optimization is decoupled for determining the α_{mnl}. The optimization steps are similar to minimization in the concentration field. The inequality becomes an equality if $u_{des,MNL}$ is a Fourier sine series or a Fourier cosine series. Finally, $\alpha(x,y,z)$ is constructed by

$$\alpha(x,y,z) = \sum_{-MNL}^{MNL} \alpha_{mnl} e^{(m\pi x + n\pi y + l\pi z)i}. \tag{73}$$

5.3. *Case II:* $k_p \neq 0$

As before, replace $C(x,y,z,t)$ by $C_d(x,y,z,t)$ in the PDE to obtain

$$u_{MNL}(x,y,z,t) = \alpha_{MNL}(x,y,z) w(t) + \delta \sum_{j=1}^{\infty} (j\pi)^2 \int_0^t C_{d,MNL}(x,y,z,\tau) e^{-\gamma j^2 \pi^2 (t-\tau)} d\tau, \tag{74}$$

where δ is defined in (48), and

$$C_{d,MNL}(x,y,z,t) = \sum_{-MNL}^{MNL} c_{d,mnl} e^{(m\pi x + n\pi y + l\pi z)i}, \tag{75}$$

$$c_{d,mnl} = \int_\Omega C_d(x,y,z,t) e^{-(m\pi x + n\pi y + l\pi z)i} \, dV. \tag{76}$$

DOI: 10.1002/oca

With the time shift,

$$\int_{t_0}^{t_f}\int_{\Omega}\left(\sum_{-MNL}^{MNL}\left(u_{des,mnl}(t)-\alpha_{mnl}w(t-t_p)-\delta\sum_{j=1}^{\infty}(j\pi)^2\int_0^t c_{d,mnl}(\tau)e^{-\gamma j^2\pi^2(t-\tau)}d\tau\right)e^{-(m\pi x+n\pi y+l\pi z)i}\right)^2 dVdt$$

$$\leqslant\sum_{-MNL}^{MNL}\int_{t_0}^{t_f}\left(u_{des,mnl}(t)-\alpha_{mnl}w(t-t_p)-\delta\sum_{j=1}^{\infty}(j\pi)^2\int_0^t c_{d,mnl}(\tau)e^{-\gamma j^2\pi^2(t-\tau)}d\tau\right)^2 dt. \quad (77)$$

The optimization is decoupled for determining α_{mnl}, and the optimization steps are similar to minimization in the concentration field.

6. NUMERICAL EXAMPLE

Consider the spatial field control problem (24) with the dimensionless constants $D = 1$, $k = 0.1$, $v = 0$, and the reference field

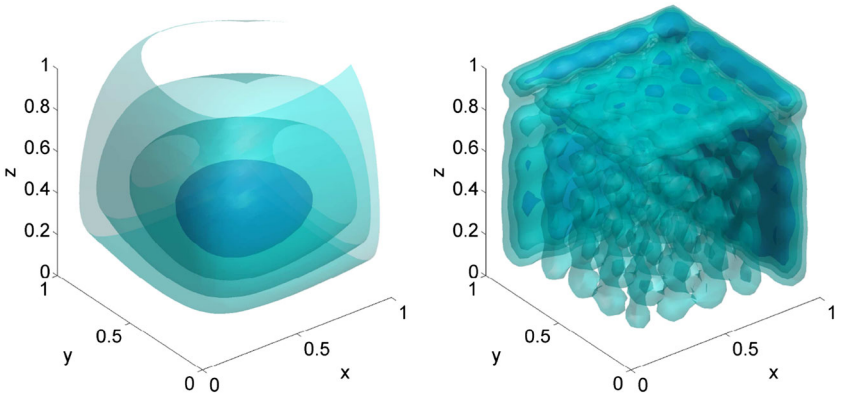

Figure 2. (Left) Reference field showing isosurfaces of 0.01, 0.008, 0.006, and 0.004 from inside to outside at $t = 0.7$. (Right) Optimal $\alpha(x, y, z)$ for the microparticles showing isosurfaces of 16, 12, 8, and 4 from inside to outside for $M = N = L = 10$.

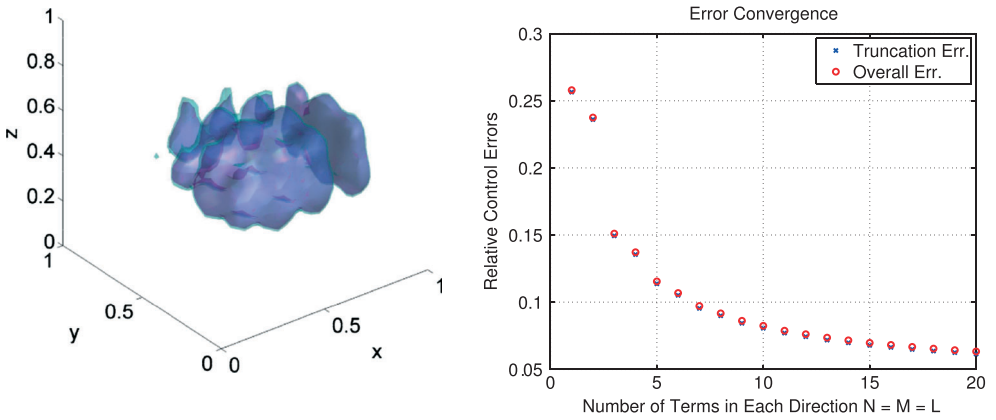

Figure 3. (Left) Approximated reference (magenta) and optimal concentration (cyan) fields for $M = N = L = 10$ showing the isosurface of 0.01 at $t = 0.7$. (Right) The minimum control error (41) is the red circles, the second term in (41) is the blue crosses, and both are plotted relative to the error 5.45×10^{-5}, which is the case when no molecules are released.

DOI: 10.1002/oca

$$C_d(x, y, z, t) = \left(e^{-x} - e^{-3x}\right)\left(e^{-y} - e^{-4y}\right)\left(e^{-2z} - e^{-4z}\right)\left(e^{-t} - e^{-2t}\right). \tag{78}$$

The manufacturing process that places microparticles within the 3D tissue scaffold is the most efficient when the spatial variation in the initial loading in the microparticles is constrained to low frequencies. First consider the objective of determining the optimal microparticle properties (25) when the maximum spatial frequency in any spatial direction is 10π ($M = N = L = 10$).

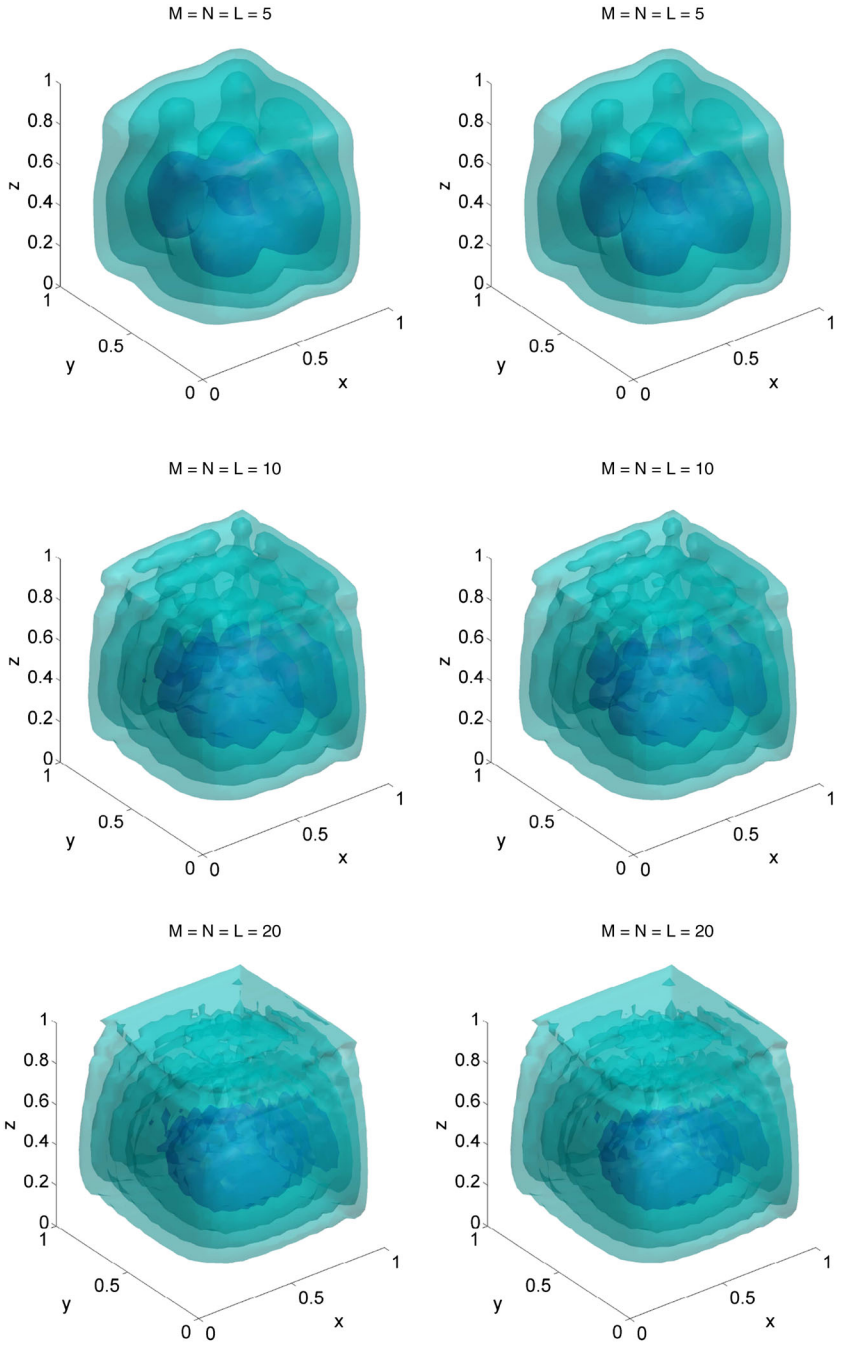

Figure 4. Optimal (left column) and approximated reference (right column) concentration fields showing isosurfaces of 0.01, 0.008, 0.006, and 0.004 from inside to outside at $t = 0.7$ and the minimum control error, for varying number of basis functions.

DOI: 10.1002/oca

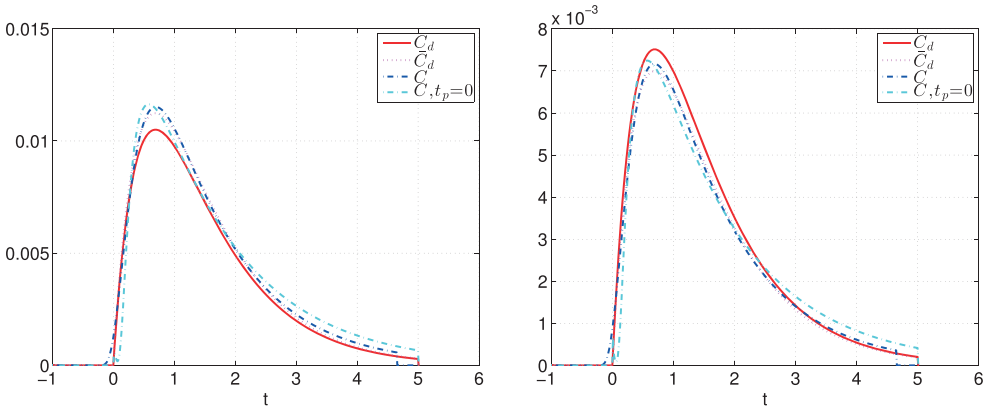

Figure 5. Reference C_d, approximate (truncated) reference $\bar{C}_d$, and optimal concentration profiles C at the center position ($x = y = z = 1/2$, left) and at an off-center position ($x = y = z = 1/4$, right) for $M = N = L = 10$.

Figure 2 shows the reference field C_d (78) at a representative time. The optimal properties of the microparticles are

$$\{r_p/R_p, \kappa/R_p^2, t_p\} = \{0.48, 0.08, -0.20\} \tag{79}$$

with $\alpha(x, y, x)$, which is proportional to the optimal initial loading, shown in Figure 2 (right). The negative trigger time t_p indicates that the core-shell microparticles should be activated before the given C_d is initiated, which is possible because the desired uptake rate is known a priori. The number density ρ and initial loading $C_{r0}(x, y, z)$ of the core-shell microparticles appear as a product in $\alpha(x, y, x)$, so that the extra degree of freedom can be used to simplify manufacturing. For example, for a fixed optimal $\alpha(x, y, x)$, the number density ρ could be reduced so that fewer microparticles would need to be positioned in a 3D tissue scaffold, by increasing the initial loading. Similarly, the effective diffusion coefficient κ and radius R_p of the microparticles affect the molecular species release through the inverse time scale κ/R_p^2, so this extra degree of freedom can also be used to simplify manufacturing. By manufacturing to specify the pore size, the porous polymer microparticles can be made with κ having any specified value from arbitrarily small to nearly the value of the effective diffusion coefficient D. This flexibility can be used to select the microparticle radius R_p small enough that the initial loading $C_{r0}(x, y, z)$ and concentration in the model (16) behave like a continuum ($R_p \ll 1/\max\{M, N, L\}$). For example, $\kappa/R_p^2 = 0.08$ could be obtained by selecting $R_p = 0.01 \ll 1/10$, which is small enough to spatially resolve the initial loading, and selecting $\kappa = 0.08(0.01)^2 = 8 \times 10^{-6}$, which can be implemented by using very small pore diameters in the polymeric microparticles.

The spatial complexity of the optimal initial loading in Figure 2 indicates that it is unlikely that a person would be able to design the optimal initial loading by intuition,[§] which motivates the application of numerical optimization. The concentration field obtained with optimal polymer microparticles is nearly indistinguishable from the approximated reference field $\bar{C}_d$ (truncated sum of (39)), indicating that the microparticles provide a very high degree of controllability within the constraint on the spatial resolution (see Figure 3).

If the microparticles can be spaced more closely together, then M, N, and L increase, and the differences between the optimal and reference fields become smaller (compare Figure 4 with Figure 2). These differences vary with position. For example, the optimal concentration is mostly higher than the reference for the center of the spatial domain but mostly lower than the reference for the off-center position $x = y = z = 1/4$ (see Figure 5).

Zeroing the trigger time increases the minimum control error (24) by a factor of 7, indicating that the trigger time is a useful optimization variable. Although the respective optimal concentration fields look similar at first glance (see Figure 5), the zero trigger time is associated with

[§]The optimal initial loading is much smaller in the center of the spatial domain than in the surrounding region.

DOI: 10.1002/oca

an initial concentration increase at $t = 0$ that is less sharp, which is the primary contribution to the control error. A tissue engineer would have to assess whether the improvement in tracking the 3D concentration field is worth the extra experimental effort of implementing an environmental trigger.

7. CONCLUSIONS

This article is the first (other than a related conference paper) to explicitly account for the dynamics within polymer microparticles while optimizing their spatial and temporal release of macromolecules within an engineered tissue construct. With its incorporation of state constraints in the form of PDEs for the microparticles and limitations on spatial frequencies, the mathematical formulation for the spatial field control problem is significantly more sophisticated than spatial field control problems described in the literature. Spectral decomposition was a useful approach for direct satisfaction of the spatial frequency constraints and reduction of the large number of degrees of freedom in the optimization problem. In the simulation results, the control error was mostly due to the limitation on the spatial resolution, which can be overcome by using smaller microparticles spaced more closely together.

Several directions are promising for future work. Microparticles of different design such as microcapsules or particles constructed with biodegradable polymers could be investigated. Nonlinear cellular uptake kinetics, molecular degradation kinetics, and molecular interactions with the extracellular matrix are also of practical importance. The ultimate objective of this research is to develop a suite of mathematical tools for controlling the spatial and temporal development of an engineered tissue construct that can be used to guide experimental designs and reduce trial-and-error experimentation.

ACKNOWLEDGEMENTS

The authors thank David Mooney, Xuanhe Zhao, Nathaniel Huebsch, and Erin Anderson at Harvard University for critiques of the tissue engineering model, and David Mooney for hosting the sabbatical of Richard D. Braatz during which part of this paper was written. Financial support is acknowledged from the National Institutes of Health NIBIB 5RO1EB005181 and the National Science Foundation (Grant #0426328).

REFERENCES

1. Kishida M, Pack DW, Braatz RD. State-constrained optimal spatial field control for controlled release in tissue engineering. *Proceedings of the American Control Conference*, Baltimore, MD, USA, 2010; 4361–4366.
2. Hargrove JW. Optimized simulation of the control of tsetse flies Gloissina pallidipes and G.m. morsitans (Diptera : Glossinidae) using odour-baited targets in Zimbabwe. *Bulletin of Entomological Research* 2003; **93**:19–29.
3. Kishida M, Versypt ANF, Pack DW, Braatz RD. Optimal control of one-dimensional cellular uptake in tissue engineering. *Optimal Control Applications and Methods* 2013; **34**:680–695.
4. Stephanou A, McDougall SR, Anderson ARA, Chaplain MAJ. Mathematical modelling of flow in 2D and 3D vascular networks: applications to anti-angiogenic and chemotherapeutic drug strategies. *Mathematical & Computer Modelling* 2005; **41**(10):1137–1156.
5. Smyshlyaev A, Krstic M. On control design for PDEs with space-dependent diffusivity or time-dependent reactivity. *Automatica* 2005; **41**:1601–1608.
6. Bensoussan A, Prato GD, Delfour MC, Mitter SK. *Representation and Control of Infinite Dimensional Systems* (2nd edn). Birkhauser: Boston, 2007.
7. Lasiecka I, Triggiani R. *Control Theory for Partial Differential Equations: Continuous and Approximation Theories I - Abstract Parabolic Systems*. Cambridge University Press: Cambridge, U.K., 2000.
8. Lasiecka I, Triggiani R. *Control Theory for Partial Differential Equations: Continuous and Approximation Theories II – Abstract Hyperbolic-like Systems over a Finite Time Horizon*. Cambridge University Press: Cambridge, U.K., 2000.
9. Nagy ZK, Braatz RD. Open-loop and closed-loop robust optimal control of batch processes using distributional and worst-case analysis. *Journal of Process Control* 2004; **14**:411–422.
10. Ray WH. *Advanced Process Control*. McGraw-Hill: New York, 1980.
11. Betts JT, Campbell SL, Engelsone A. Direct transcription of optimal control problems with high order state constraints: theory vs. practice. *Optimization and Engineering* 2007; **8**:1–19.

DOI: 10.1002/oca

12. Kameswaran S, Biegler LT. Advantages of nonlinear-programming-based methodologies for inequality path-constrained optimal control problems – a numerical study. *SIAM Journal on Scientific Computing* 2007; **30**: 957–981.
13. Featherstone AP, Braatz RD. Control-oriented modeling of sheet and film processes. *AIChE Journal* 1997; **43**: 1989–2001.
14. Kishida M, Braatz RD. Optimal spatial field control of distributed parameter systems. *Proceedings of the American Control Conference*, St. Louis, MO, USA, 2009; 32–37.
15. Luenberger DG. *Optimization by Vector Space Methods*. Wiley: New York, 1997.
16. Blatt M, Schittkowski K. Optimal control of one-dimensional partial differential algebraic equations with applications. *Annals of Operations Research* 2000; **98**:45–64.
17. Kishida M, Braatz R D. RBF-based 2D optimal spatial control of the 3D reaction–convection–diffusion equation. *Proceedings of the European Control Conference*, Budapest, Hungary, 2009; 1949–1954.
18. Kunisch K, Volkwein S. Control of the Burgers equation by a reduced-order approach using proper orthogonal decomposition. *Journal of Optimization Theory & Applications* 1999; **102**:345–371.
19. Lall S, Marsden JE, Glavaski S. A subspace approach to balanced truncation for model reduction of nonlinear control systems. *International Journal of Robust and Nonlinear Control* 2002; **12**:519–535.
20. Ly H V, Tran H T. Modeling and control of physical processes using proper orthogonal decomposition. *Mathematical & Computer Modelling* 2001; **33**:223–236.
21. Chen RR, Mooney DJ. Polymeric growth factor delivery strategies for tissue engineering. *Pharmaceutical Research* 2003; **20**:1103–1112.
22. Mahoney MJ, Saltzman WM. Controlled release of proteins to tissue transplants for the treatment of neurodegenerative disorders. *Journal of Pharmaceutical Sciences* 1996; **85**:1276–1281.
23. Mahoney MJ, Saltzman WM. Transplantation of brain cells assembled around a programmable synthetic microenvironment. *Nature Biotechnology* 2001; **19**:934–939.
24. Richardson TP, Peters MC, Ennett AB, Mooney DJ. Polymeric system for dual growth factor delivery. *Nature Biotech.* 2001; **19**:1029–1034.
25. Saltzman WM, Olbricht WL. Building drug delivery into tissue engineering. *Nature Reviews Drug Discovery* 2002; **1**:177–186.
26. Berkland C, Pollauf E, Pack DW, Kim K. Uniform double-walled polymer microspheres of controllable shell thickness. *Journal of Controlled Release* 2004; **96**:101–111.
27. Varde NK, Pack DW. Microspheres for controlled release drug delivery. *Expert Opinion on Biological Therapy* 2004; **4**:35–51.
28. Cussler EL. *Diffusion* (2nd edn). Cambridge University Press: U.K., 1997.
29. Byrne ME, Salian V. Molecular imprinting within hydrogels II: progress and analysis of the field. *International Journal of Pharmaceutics* 2008; **364**:188–212.
30. Kost J, Leong K, Langer R. Ultrasound-enhanced polymer degradation and release of incorporated substances. *PNAS* 1989; **86**:7663–7666.
31. Peppas NA, Buresa P, Leobandunga W, Ichikawab H. Hydrogels in pharmaceutical formulations. *European Journal of Pharmaceutics and Biopharmaceutics* 2000; **50**:27–46.
32. Qiu Y, Park K. Environment-sensitive hydrogels for drug delivery. *Advanced Drug Delivery Reviews* 2001; **53**: 321–339.
33. Sakiyama-Elbert SE, Hubbell JA. Development of fibrin derivatives for controlled release of heparin-binding growth factors. *Journal of Controlled Release* 2000; **65**:389–402.
34. Cima LG, Cima MJ. Tissue regeneration matrices by solid free form fabrication techniques, 1996. US Patent 5518680.
35. Mapili G, Lu Y, Chen SC, Roy K. Laser-layered microfabrication of spatially patterned functionalized tissue-engineering scaffolds. *Journal of Biomedical Materials Research Part B* 2005; **75B**:414–424.
36. Cereijido M, Rotunno CA. *Introduction to the Study of Biological Membranes*. Gordon and Breach Science Publishers: New York, 1970.
37. Truskey GA, Yuan F, Katz DF. *Transport Phenomena in Biological Systems*. Prentice Hall: Upper Saddle River, NJ, 2004.
38. Polyanin AD. *Handbook of Linear Partial Differential Equations for Engineers and Scientists*. Chapman & Hall/CRC: Boca Raton, FL, 2001.
39. Deen WM. *Analysis of Transport Phenomena*. Oxford University Press: New York, 1998.
40. Flyer N, Swarztrauber PN. The convergence of spectral and finite difference methods for initial-boundary value problems. *SIAM Journal on Scientific Computing* 2002; **23**:1731–1751.

DOI: 10.1002/oca